Understanding the Performance Limiting Factors of $Cs_2AgBiBr_6$ Double-Perovskite Solar Cells

Giulia Longo,[‡†] Suhas Mahesh,[†] Leonardo R. V. Buizza,[†] Adam D. Wright,[†] Alexandra J. Ramadan,[†] Mojtaba Abdi-Jalebi,[□ǂ] Pabitra K. Nayak,[#] Laura M. Herz,[†] Henry J. Snaith[†]

‡ Department of Mathematics, Physics and Electrical Engineering, Northumbria University, Ellison place, Newcastle upon Tyne, NE18ST, United Kingdom

† Clarendon Laboratory, Department of Physics, University of Oxford, Parks Road, Oxford, OX13PU, United Kingdom

□ Institute for Material Discovery, University College London, Torrington Place, London, WC1E 7JE, United Kingdom

ǂ Cavendish Laboratory, Department of Physics, University of Cambridge, JJ Thomson Avenue, Cambridge CB3 0HE, United Kingdom

[#] TIFR Centre for Interdisciplinary Sciences, Tata Institute of Fundamental Research, Hyderabad, 500107, India

Corresponding authors

*Giulia Longo g.longo@northumbria.ac.uk

*Henry J Snaith henry.snaith@physics.ox.ac.uk

ABSTRACT

Double-perovskites have recently emerged as possible alternatives to lead-based halide perovskites for photovoltaic applications. In particular, $Cs_2AgBiBr_6$ has been the subject of several studies due to its environmental stability, low toxicity, and its promising optoelectronic features. Despite these encouraging features, the performances of solar cells based on this double-perovskite are still low, suggesting severe limitations that need to be addressed. In this work we combine experimental and theoretical studies to show that the short electron diffusion length is one of the major causes for the limited performances of $Cs_2AgBiBr_6$ solar cells. Using EQE measurements on semi-transparent $Cs_2AgBiBr_6$ solar cells, we estimate the electron diffusion length to be only 30 nm and corroborated this value by THz spectroscopy. By using of photothermal deflection spectroscopy and surface photovoltage measurements we correlate the limited electron diffusion length with a high density of electron traps. Our findings highlight important faults affecting this double-perovskite, showing the challenges to overcome and hinting to a possible path to improve the efficiency of $Cs_2AgBiBr_6$ solar cells.

In the last decade, organic-inorganic lead-halide perovskites have been the protagonists of a remarkable ascent in the photovoltaic landscape, with the power conversion efficiency of single-junction solar cells skyrocketing to 25.2% in less than 10 years of investigation, and over 29% when integrated into tandem cells with silicon.[1] Despite the impressive photovoltaic performance, these hybrid materials present some drawbacks. In fact, even the best perovskite-based cells currently have much lower operating lifetimes in the ambient (thousands of hours)[2] than traditional inorganic semiconductor based cells (~25 years). The volatility of the organic cation is considered to be a significant contributor to this instability,[3,4] which should be improved using inorganic cations. However, attempts to utilize the inorganic perovskite $CsPbI_3$

have been thwarted by the intrinsic thermodynamic instability of the photoactive phase at room temperature.[5,6] Additionally, there are some concerns due to the presence of lead, as well as the almost exclusive use of toxic solvents in solution processing. While studies thus far have indicated that the associated risk of the use of lead is small, when deployed in utility scale solar,[2,7,8] social barriers towards the use of lead may need to be addressed.[9] Furthermore, there may simply be other materials which are yet to be discovered, which could have superior properties than lead-halide perovskites. For these reasons, the search for alternative inorganic perovskites employing less toxic metals is of high interest. The flexible perovskite crystal structure admits a staggering number of elements with wide variety of configurations[10] and therefore represents an ideal set where to conduct this search. The model perovskite should retain the near-ideal optoelectronic properties (long diffusion length, low trap density, direct-bandgap ideally between 1-1.8 eV).

In this landscape, double-perovskites have recently emerged as particularly promising alternatives[11-13] exhibiting encouraging optoelectronic properties, high environmental stability and low toxicity. In the double-perovskite crystal, Pb^{2+} is replaced by alternating monovalent and trivalent metal cations, thus preserving an average divalency. The resulting three-dimensional structure takes the form $A_2M'M''X_6$, where A is a monovalent cation, M' and M'' are monovalent and trivalent metal ions respectively, and X is a halide anion. Initial computational studies pointed to pnictogens (Bi^{3+} and Sb^{3+}) and noble metals (Cu^{+}, Ag^{+}, Au^{+}) as optimal substitutes for Pb^{2+}, due to their stable oxidation states, high conductivity in the metallic form, and ionic radii comparable to Pb^{2+} in an octahedral environment.[14,15] Recent works on the $Cs_2M'M''X_6$ family (M'=Au^{+}, Ag^{+}, Cu^{+} and M''=Bi^{3+}, Sb^{3+}) have revealed encouraging optoelectronic properties, characterized by visible to near infrared absorption,[16-18] relatively small carrier effective mass[14] and bright emission.[19,20]

In particular, the double-perovskite $Cs_2AgBiBr_6$ has been the subject of much fundamental material characterisation and initial application in photodetectors and photovoltaic devices.[11,16,18,21-25] Material characterisation and calculations suggest promising features: single-crystal carrier lifetime of 1 μs, moderate charge-carrier mobility, and an absorption-edge in the visible.[26] However, despite these favourable characteristics, the best reported photovoltaic power conversion efficiency (PCE) for a planar heterojunction solar cell is still only 2.84%, with an open circuit voltage (V_{OC}) of 1.06 V, fill factor (FF) of 0.524 and short-circuit current (J_{SC}) of 5.13 mA cm^{-2}.[25] It is historically common that incipient PV technologies suffer from large voltage deficits, which gradually reduce as material processing improves and as methods to passivate defects are discovered.[27] However, the severely inhibited J_{SC} is unusual, and could prove to be a major barrier to high performance. Furthermore, due to the indirect bandgap of $Cs_2AgBiBr_6$, thick absorber films, on the order of tens to hundreds of microns, would be necessary to substantially increase the photocurrent generation, but this would require extremely long charge-carrier diffusion lengths. For this reason, knowing the charge-carrier mobility and diffusion length is fundamental to choose the proper material thickness for high short-circuit currents. Notwithstanding this, a clear evaluation of these parameters in this material is still missing, and to date, several different values have been reported.[26,28-31]

Here, we undertake a thickness-dependent study of vapour deposited $Cs_2AgBiBr_6$–based solar cells. We evaluate the carrier diffusion length based on the combination of external quantum efficiency (EQE) measurements on semi-transparent devices and optical modelling, and compare it to values we estimate using terahertz photoconductivity spectroscopy and time resolved photoluminescence. We specifically reveal that short electron diffusion length, on the order of a few tens of nanometers, is the cause for low short-circuit current densities reported in these solar cells. We also perform photo-thermal deflection spectroscopy (PDS) and surface photovoltage measurements (SPV) and correlate this short electron diffusion length with the

presence of a high density of electron traps. We suggest that the electron diffusion lengths in $Cs_2AgBiBr_6$ must be improved as a matter of priority, in order to achieve better performance. Such improvements, likely driven by reduction in trap densities, would also increase open-circuit voltages and reduce hysteresis.

In this work we prepare $Cs_2AgBiBr_6$ thin films through sequential evaporation, as described in the Supporting Information. To assess the successful formation of the double-perovskite, we performed X-Ray diffraction (XRD) of thin-films deposited on FTO. The sharp peaks in the XRD pattern (Figure 1a) of the evaporated material confirm its high crystallinity and the absence of any additional phases or unreacted precursors. Optical properties measured on a quartz substrate (absorbance, photoluminescence -PL- spectra, photoluminescence excitation -PLE- spectra) are presented in Figure 1b, and are consistent with previous reports.[16,32,33] The films exhibit strong and increasing absorption below 400 nm, which has been identified with the direct-bandgap at ~ 3 eV. The strong peak at 440 nm is still subject of controversy: some identify it with a tightly bound exciton at the direct bandgap edge,[34,35] while others ascribe it to a strong transition between the Bi^{3+} s-p orbitals, without bound character.[36,37] The weak absorption tail beyond 440 nm is considered to be the indirect bandgap, which we will return to later on. The large Stokes shift between absorption and emission, the similarity between the absorption and PLE spectra, and the independence of the PLE spectra from the emission wavelength at which are measured (Figure S1), are common signal of charge-lattice interaction mechanisms, like polaron formation, self-trapped excitons or colour-centre formations, as previously reported in other works.[20,24,38-40] We note that recently Zelewski et al. observed a "quenching" of the PLE spectra of $Cs_2AgBiBr_6$ single crystals, for excitations around 2.8 eV (440 nm). We cannot observe this same quenching in the thin films here, except for the weak emission detected at shorter wavelengths than 520 nm (Figure S1). It is beyond the scope of our present work to investigate further into this phenomenon, but we highlight that ambiguities

around the whole nature of photoexcitation and emission in this material still persist.

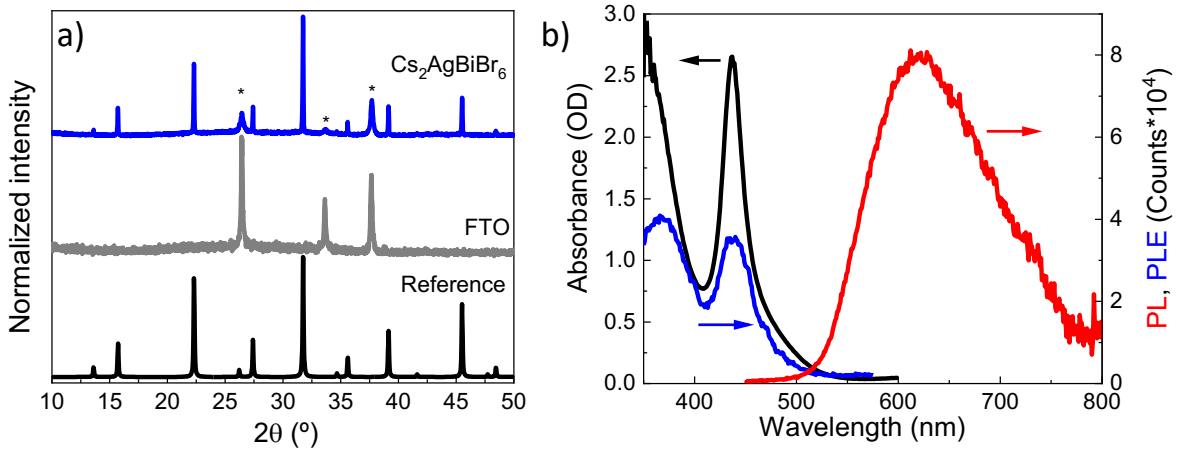

Figure 1 a) XRD pattern of the evaporated and annealed $Cs_2AgBiBr_6$ thin-film on FTO. b) Absorption (black curve), PL excitation spectrum (PLE, blue curve, recorded at 600 nm emission peak) and PL spectrum (red curve, excitation at 405 nm) of $Cs_2AgBiBr_6$ thin-film deposited on quartz.

We then prepared double-perovskite n-i-p cells with different active layer thicknesses. The structure of the fabricated n-i-p cell is FTO/TiO_2 /$Cs_2AgBiBr_6$/Spiro-OMeTAD/Ag, as described in the Supporting Information and schematically represented in Figure S2a. In Figure 2a we present the JV curves of the best devices for each film thickness, while in Figure S2b we present the corresponding steady-state J_{SC} and steady-state power output (SPO) which are similar to those obtained from voltage scans (Table S1). The champion device, obtained with 750 nm of double-perovskite active layer, was measured to have a PCE of 1.03%, with an open-circuit voltage (V_{OC}) of 1.10 V, short-circuit current (J_{SC}) of 1.33 mA cm^{-2} and a fill-factor (FF) of 0.70, which are comparable to previous reports.[41-43] Interestingly, we do not observe any clear trend between the device performance and the active layer thickness, as Figure 2b reveals. We show the XRD patterns of perovskite layers of different thickness in Figure S2c, which exclude the possibility of unwanted phases or unreacted precursors in the different films.

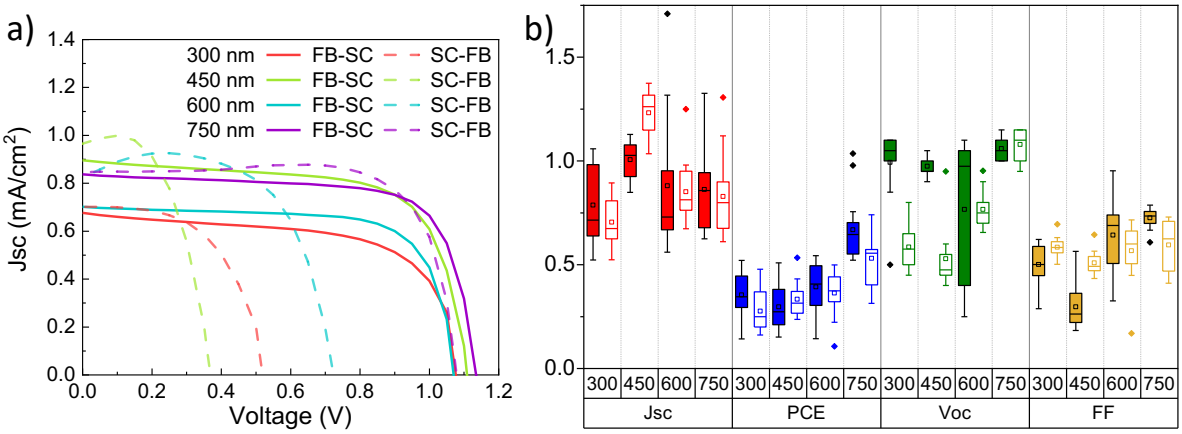

Figure 2 a) J-V curves of the solar cells with different $Cs_2AgBiBr_6$. b) J_{SC} (mA/cm^2, red), PCE (%, blue), V_{OC} (V, green) and FF (yellow) of 15 cells for each $Cs_2AgBiBr_6$ thickness. Forward-bias to short-circuit (FB-SC) scans and data are shown as solid-lines and filled bars, and short-circuit to forward bias (SC-FB) scans and data as dashed lines and open bars.

In the inset to Figure 3a, we show a Tauc plot of the absorption spectra, from which we determine an indirect bandgap at 2.25 eV, similar to previous reports.[14,16] . For such a material, the thermodynamic limit, for the performance (with the Shockley-Queisser assumptions[44]) would be 17.6%, with V_{OC} =1.93 V and J_{SC} =9.79 mA cm^{-2}. Every 60 mV loss in V_{OC} from the thermodynamic limit, corresponds to an order-of-magnitude reduction in the external radiative efficiency (ERE).[45-47] Our devices exhibit a large voltage deficit of ~800 mV, suggesting an extremely low external radiative efficiency (ERE) of ~10^{-13} for a full device with injection condition comparable to 1 sun. In comparison, the best inorganic-organic perovskite cells have ERE~0.1. This is indicative of an extremely high rate of non-radiative recombination, which in turn indicates extremely large trap densities or other non-radiative processes. We investigate the sub band gap absorption in these thin films via photothermal deflection optical absorption spectroscopy (PDS, Figure 3a). This observation reveals a shallow absorption edge with an Urbach energy of 70 meV, and significant "panchromatic" absorption, at between 1% and 0.1%

of the peak absorption strength, reaching down to 1000 nm. This is consistent with a large density of sub-bandgap states, which we would expect to mediate fast charge-carrier trapping and subsequent non-radiative recombination. We measured the PL quantum yield (PLQY), of our neat $Cs_2AgBiBr_6$ thin films on glass (Figure 3b), determining a value of ~0.08% (~10^{-4}). Although this PLQY value is low, as compared to lead halide perovskites, it is orders of magnitude higher than the 10^{-13} required to justify such low Voc in the solar cells assuming a Shockley-Queisser type step function absorption spectrum. However, even in the radiative limit, the shallow absorption onset and the presence of such sub-bandgap states can be expected to significantly limit the open-circuit voltage in PV devices. This is due to the dark recombination current density (J_0) being proportional to the overlap integral of the black body spectrum under ambient temperature (300 K), and the absorption spectrum of the solar absorber material. Since the 300 K black body spectrum increases exponentially moving towards lower energy, this factor, J_0, is highly sensitive to small changes in both the steepness of the absorption onset (Urbach energy) and sub band gap absorptions.[27] Furthermore, charge quenching at the interface between the absorber layer and the charge extraction layer is also usually responsible for significantly quenching the luminescence efficiency in a lead-halide perovskite PV cells.[48] This is specifically problematic for wider band gap absorber materials,[47] where there has been little work thus far appropriately matching the energetics at these interfaces. Therefore, further improvement in Voc is likely to be feasible via better election of materials for charge extraction layer, or tuning of this interface to minimise recombination losses. Historically, PV technologies started off with hundreds of mV of voltage deficit, which slowly improved as materials processing and device architecture design improved. However, the very low photocurrent density, representing a loss of ~ 90% of the absorbed photons, is not typical, even for incipient materials. Consequently, we must consider what can be the origin of these photocurrent losses.

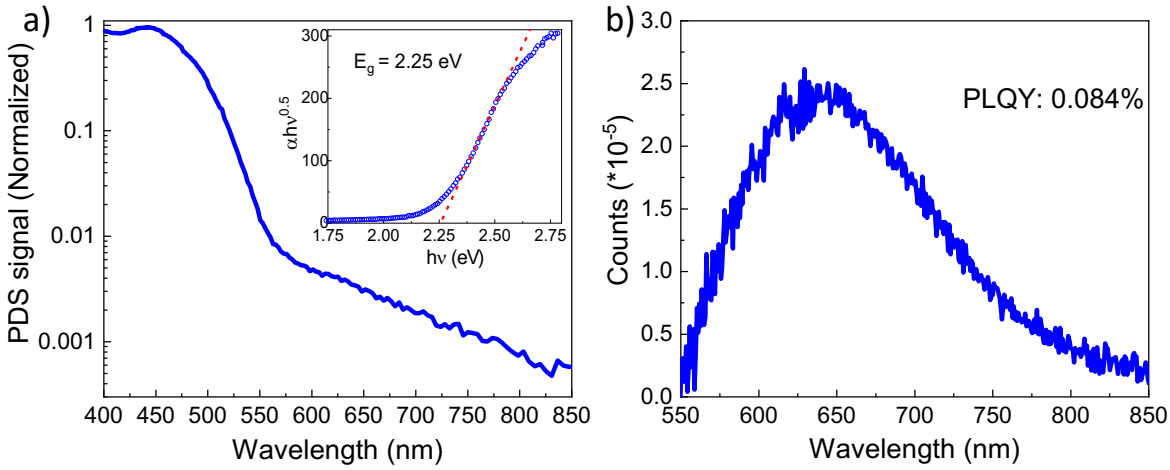

Figure 3 a) PDS spectrum of neat $Cs_2AgBiBr_6$ film on quartz glass. Inset, Tauc plot with the calculated indirect bandgap reported. b) PL spectrum and PLQY value of $Cs_2AgBiBr_6$ measured in an integrating sphere with 405nm laser excitation.

To answer this question, we investigate the charge transport and photocurrent generation in complete $Cs_2AgBiBr_6$ solar cells and thin film in order to estimate the carrier diffusion lengths and reveal if there exists an asymmetry in the electron and hole conduction out of the device. We first fabricated semi-transparent PV cells with 435 nm of $Cs_2AgBiBr_6$, and measured their photovoltaic external quantum efficiency (EQE) spectra through front illumination (through the *n* side), and rear illumination (through the *p* side), which we schematically represent in Figure 4a. When illuminated through the *n* side, the EQE (blue curve in Figure 4b) has a peak of ~15%, which very closely matches the absorption spectrum in shape, and has an air-mass (AM) 1.5 integrated current of 0.78 mA cm^{-2}. When illuminated through the *p* side, the EQE (orange curve in Figure 4b) peaks at only 2.5%, has a shape that counter-correlates with the absorption spectrum, and gives an AM1.5 integrated current of 0.16 mA cm^{-2}. We note that the light attenuation from the 20 nm thick "semi-transparent" gold (~20% at 450 nm) is not sufficient to account for this effect. To understand these results, we have to consider that as light passes through the perovskite, its intensity decays exponentially with depth accordingly

to the Beer-Lambert law. This means that the density of generated carriers will be higher closer to the transport layer from which light enters in the device (*i.e.*, higher density next to the electron-transport layer (ETL) for *n* side illumination, and higher density close to the hole-transport layer (HTL) for *p* side illumination, as represented by the carrier generation profile curves in Figure 4a). Consequently, with the *n* side illumination, holes will have the longer path to travel to be extracted, as compared to electrons, while for *p* side illumination electrons will have to travel further than holes to reach the ETL, as indicated by the open-arrows in Figure 4a. Observing the EQE in Figure 4b, it is clear that the *p* side EQE is much lower than the *n* side EQE, indicating that when electrons have to travel across the entire active layer thickness, they cannot be efficiently collected. Furthermore, the *p* side EQE also shows an "inversion" in shape in comparison to the *n* side EQE and to the absorption spectrum: the peak in the absorption at 440 nm corresponds to a dip in the *p* side EQE. This happens because wavelengths that are strongly absorbed do not reach the far-end (electron-transporting layer in this case), causing a dip. Weakly absorbed wavelengths, instead, propagate to the far end in greater numbers, appearing as peaks. In contrast, the *n* side EQE spectrum very closely follows the absorption spectra, with the clearly defined peak at 440 nm, rather than the total absorptance spectrum, which for this 435 nm thick film is much broader, as we illustrate in Figure S3. This observation is consistent with only a very thin section of the film near the electron extraction layer contributing to photocurrent generation.

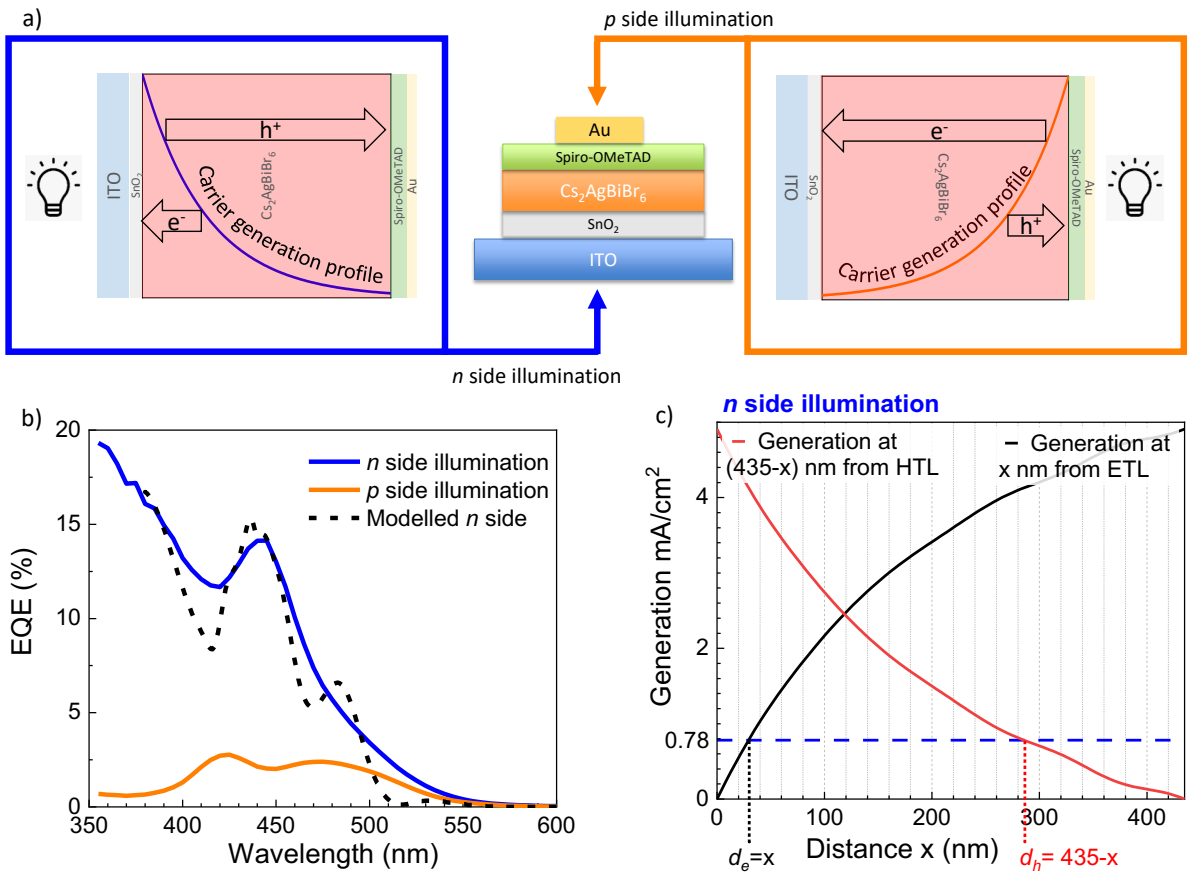

Figure 4 a) Schematic illustration of the device structure used in the double-side EQE measurement and the two measurement conditions, with the corresponding carrier generation profile. b) EQE measured with illumination from the ITO (blue curve), from the gold (orange curve) and the modelled n-EQE (black dashed curve). c) Current generation at a distance x from the ETL (black curve) and from a distance 435-x from the HTL (red curve) in the case of n-side illumination. The dotted blue line indicates the current obtained from the integration of the n-EQE

These considerations lead us to conclude that electron diffusion is the factor limiting the short-circuit current of $Cs_2AgBiBr_6$ solar cells. We then combined our EQE data with an optical model (generalised transfer matrix method) to obtain a quantitative estimation of the electron and hole diffusion length in our devices (Figure 4c). For this, we made the following simplified

consideration; if the diffusion length of electrons is d_e, we assume that only electrons generated within a length d_e from the ETL will be collected. We make the same assumption for the diffusion length of holes d_h, and undertake that the overall short-circuit current in the device will be governed by the smaller of the electron and hole currents. We then modelled the carrier generation profile as a function of incident light wavelength using the generalised transfer matrix method, and estimated the total light absorbed as a function of wavelength within a length d of a transport layer. This allowed us to reconstruct the contribution to the EQE spectrum, for every section of film with thickness d, with the assumption of an abrupt interface at d; all light absorbed within d is converted to collected photocurrent, while all light absorbed beyond d is lost. Additionally, we assume that the solar cell current is limited by the smaller of the electron and hole currents. Assuming n side illumination, we varied d until the modelled EQE best approximated the measured spectrum, which we show in Figure 4b and c. This tells us that under these assumptions, the electron diffusion length d_e is ~30 nm and that the hole diffusion length $d_h > 150$nm (note greater than, not approximately). We executed the same procedure for the p side illumination (Figure S4). However, we remark that the unavailability of the optical constants of the thin gold semi-transparent electrode causes an underestimation in the EQE modelled for p side illumination. We also note that the interference fringes visible in our modelled EQE spectrum (Figure 4b), which are not replicated in the experimental data, are likely to reflect that the physical material interfaces are not perfectly smooth in the real devices, as required for coherent optical interference.

To further investigate charge-carrier mobility, and to corroborate the above estimated carrier diffusion lengths (d_e ~30nm, d_h> 150nm), we performed optical-pump-terahertz-probe (OPTP) photoconductivity measurements (see the Supporting Information for a more exhaustive explanation).[28,41,49,50]

We report the results in Figure S5a. Our OPTPs measurements give a sum mobility of $\phi\Sigma\mu = 0.74 \pm 0.29$ $cm^2 V^{-1} s^{-1}$ in good agreement with previous measurements carried out by Time-Resolved Microwave Conductivity.[28] From the measured mobility we obtained the charge-carrier diffusion length by calculating the diffusion co-efficient and knowing the recombination rate, as described in the Supporting Information. In order to estimate the recombination rate, we performed time correlated single photon counting (TCSPC), and present the time resolved PL decay in Figure S5b. The highly heterogeneous nature of the PL decay has been previously reported, both in thin films and single crystals.[28,34] Fitting the PL decay using monoexponential and a stretched exponential function we obtained values for k_1 of 5–38.5*10^7 s^{-1} (see Supporting Information for the discussion on the evaluation of k_1). Approximating $R_T(n) \sim k_1$, we calculate values of 70-200 nm for the diffusion length. Although THz photoconductivity measurements cannot distinguish between electron and hole contributions to the charge-carrier mobility, providing a sum mobility, these diffusion lengths are in reasonably close agreement with the values obtained from our EQE model above. Alternatively, this mobility estimated by THz spectroscopy, is also likely to represent an upper estimate of the long-range mobility in the solar cell devices, where for the latter charge conduction is sensitive to scattering events on longer length scales.

The presence of traps states, especially at the surface and at interfaces with the extraction layers, is a common reason for short carrier lifetimes in semiconductor devices. So far we presented consistent evidence of the presence of a significant density of electron-traps in $Cs_2AgBiBr_6$. In order to gain a deeper understanding on the nature of these trap states, we performed Kelvin probe surface photovoltage (SPV) measurements on a double-perovskite thin film deposited on top of the FTO substrates and on different transport layers. Kelvin probe is a non-invasive technique that permits to evaluate the work-function of the material of interest through capacitance measurements between the sample and an oscillating tip with known

work-function. A detailed working mechanism of this technique is reported in the Supporting Information and in Figure S6. We determine the work-function of $Cs_2AgBiBr_6$ thin film deposited on FTO, measured in dark and nitrogen atmosphere, to be 4.91 eV, which is very close to the value of 4.94 eV, which we obtained from ultraviolet photoelectron spectroscopy (UPS) measurements, which are conducted under ultrahigh vacuum and presented in Figure S7. Interestingly, from UPS, we determined a deep lying valence band maximum (VBM) at around 6.8 ± 0.3 eV (see Supporting information for further discussion and discussion on error margins). Knowing that the optical bandgap is ~ 2.25 eV and assuming a negligible exciton binding energy, this indicates that we expect the position of the conduction band minimum (CBM) to be at ~ 4.55 eV. Therefore, the position of the fermi level (analogous to the work function in the KP measurements) would appear closer to the CBM, suggesting that our sequentially evaporated $Cs_2AgBiBr_6$ thin film is n-type in nature. Our result here contrasts with the previously reported works, in which this double-perovskite was presented as p-type semiconductor,[26,51,52] and also seems to be counterintuitive to our estimation of very short electron diffusion lengths, since electrons should be the majority carrier in our "n-type" material. However it is known that defect formation (and consequently the majority carrier population) are strongly influenced by the material fabrication technique that can substantially alter the semiconductor electronic properties.[53] Our results indicate that sequentially evaporated $Cs_2AgBiBr_6$ thin films present an n-type character, possibly related to Br^- vacancies[31] as has been previously infered.[24] However, we also note that UPS measurements probe the electronic structure of the utmost surface of a sample. Therefore, the presence of defects on the surface, could account for the discrepancies between our measurements and previous reports.

We present surface photovoltage (SPV) measurements of the double-perovskite films on FTO and on different transport layers in Figure 5a and b respectively.

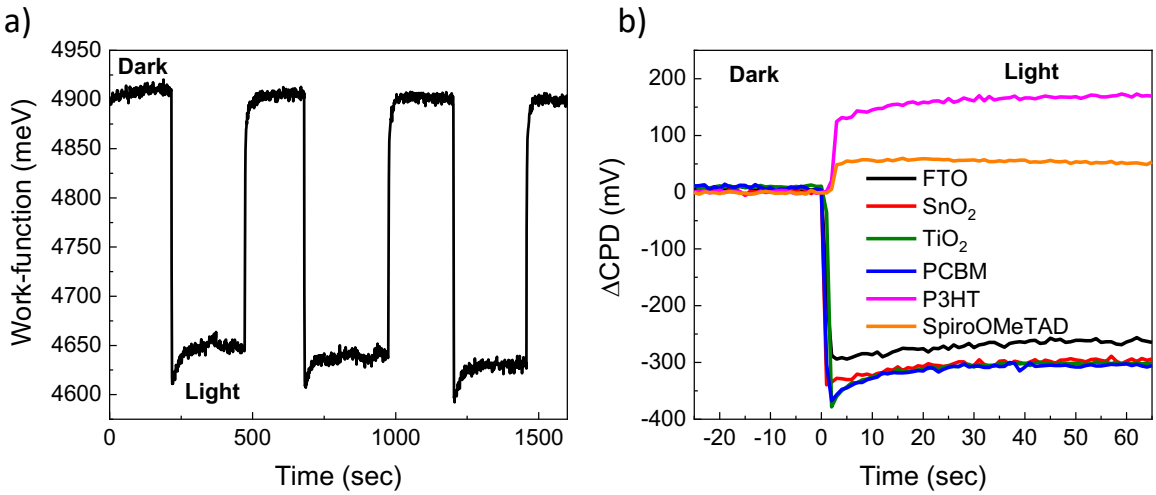

Figure 5 a) Work-function of a $Cs_2AgBiBr_6$ thin-film on FTO in dark and under white light. b) Contact potential difference of a $Cs_2AgBiBr_6$ thin-film on different charge carriers transport material.

SPV measures the change of the contact potential difference (CPD) between the sample surface and the Kelvin probe tip when the sample is illuminated, and it is defined as $SPV=CPD_{light}-CPD_{dark}$.[54] Observing the direction of the potential bending and its change with illumination, it is possible to gather information about the nature of the surface states of the semiconductor material investigated. In Figure 5a the SPV of the evaporated double-perovskite on FTO is reported. Under illumination, the work-function decreases, generating a SPV of almost -250mV. Considering the n-type character of the material, a negative SPV indicates a reduction of the band bending (see Figure S6e), consistent with the presence of electron traps. Interestingly, we observe that under illumination, the CPD (and, consequently, the calculated work-function) has an unsteady behaviour, flatting after several seconds of light exposure. The long time scale necessary for its stabilizations suggests that this phenomenon is due or influenced by a slow process, likely ionic movement. However, this behaviour is fully

recoverable, since the dark work-function value is the same even after several cycles of illumination.

Finally, we evaluate the SPV of the double-perovskite on different hole and electron transport layers (Figure 5b). All the CPD_{dark} values where set to 0 mV, in order to facilitate the comparison between the different samples. When the double-perovskite is deposited on top of electron transport materials (as SnO_2, TiO_2 or PCBM), the SPV value becomes slightly more negative than on FTO, reaching values of -300 mV. This can be understood thinking that as the free carriers are created under illumination, the electrons are selectively extracted by the transport material at the buried interface, leaving a higher hole concentration than on FTO. The holes left annihilate the trapped electron at the surface decreasing even more the band-bending. On the contrary, when a hole transport material is used as underlying layer (as Spiro or P3HT), the SPV becomes positive (+50 mV and +150 mV respectively). After photo-generation, holes get mostly extracted by the hole transport layer while electrons remain in the double-perovskite film increasing the surface band bending, then creating a positive SPV. These results are hence also consistent with the presence of electron traps at the double-perovskite surface, indicating a prevalence for electron trapping in this material

In summary, in this work, through a combined experimental and theoretical study, we have obtained a deeper understanding of the limiting factor for the performances of $Cs_2AgBiBr_6$ solar cells. A thickness-dependent study of the photovoltaic parameters of the double-perovskite devices, revealed that the J_{SC} is independent from the absorber thickness, but much lower than expected from the total light absorbed in the films. We resolved this apparent contradictory results, by analysing the EQE spectrum via illumination through the front and back side of the cells, and revealed that the material suffers from a very low electron diffusion length, but has a substantial hole-diffusion length. This observation is corroborated using THz spectroscopy, from which we determined a modest sum mobility of electrons and holes of less

than 1 $cm^2 V^{-1} s^{-1}$, and a corresponding charge carrier diffusion length of between 70 to 200nm. We ascribe this short electron diffusion length to the presence of energetic disorder and specifically a high density of electron traps, which we revealed by PDS measurements and surface photovoltage analysis. We believe that these results represent a significant step forward for understanding the deficiencies of double-perovskites for photovoltaic applications, and hence elucidate the next challenges which need to be addressed in order to improve the performances of this promising class of double-perovskites materials and optoelectronic devices.

ACKNOWLEDGMENTS

This work was funded by EPSRC through projects EP/M015254/2, EP/S516119/1, EP/M005143/1, EP/P032591/1, and by H2020 through the European Union's Horizon 2020 research and innovation programme through PERTPV project under grant agreement No 763977 and CHEOPS project under grant agreement No 730135. S.M. acknowledges funding from the Rhodes Trust (India & Worcester 2016). L.R.V.B. gives thanks to the Centre for Doctoral Training in New and Sustainable Photovoltaics and to the Oxford-Radcliffe Scholarship for financial support. P.K.N. acknowledges the support via intramural funds at TIFR Hyderabad from the Department of Atomic Energy (DAE), India. M.A.-J. thanks Cambridge Materials Limited, Wolfson College, University of Cambridge, and EPSRC for their funding and technical support.

Supporting information available: Experimental part and detailed description of the technique employed in this work. Additional graphics and tables

References

1 NREL. *Best Research-Cell Efficiencies*, <https://www.nrel.gov/pv/cell-efficiency.html> (2020).

2 Meng, L., You, J. & Yang, Y. Addressing the stability issue of perovskite solar cells for commercial applications. *Nat. Commun.* **2018**, *9*, 1-4.

3 Zhou, Y. & Zhao, Y. Chemical stability and instability of inorganic halide perovskites. *Energy Environ. Sci.* **2019,** *12*, 1495-1511.

4 Park, B.-w. & Seok, S. I. Intrinsic Instability of Inorganic–Organic Hybrid Halide Perovskite Materials. *Adv. Mater* **2019**, *31*, 1805337.

5 Eperon, G. E., Paternò G. M., Sutton, R. J., Zampetti, A., Haghighirad, A. A., Cacialli, F., Snaith H. J. Inorganic caesium lead iodide perovskite solar cells. *J. Mater. Chem. A* **2015**, *3*, 19688-19695.

6 Sharma, S., Weiden, N. & Weiss, A. in *Zeitschrift für Physikalische Chemie* Vol. 1992, *175*, 63.

7 Babayigit, A., Ethirajan, A., Muller, M. & Conings, B. Toxicity of organometal halide perovskite solar cells. *Nat. Mater* **2016**, *15*, 247-251.

8 CHEOPS EU Project, D3.1: Life Cycle Analysisof CHEOPS technologies and benchmarking: Screening, <https://www.cheops-project.eu/reports/> (**2017**).

9 CHEOPS EU Project, D3.4: Socio-economic analysis of CHEOPS technologies and benchmarking, <https://www.cheops-project.eu/reports/> (**2019**).

10 Filip, M. R. & Giustino, F. The geometric blueprint of perovskites. Proc. Natl. Acad. Sci. U. S. A. **2018**, *115*, 5397-5402.

11 Shi, Z., Guo, J., Chen, Y., Li, Q., Pan, Y., Zhang, H., Xia, Y., Huang, W., Lead-Free Organic–Inorganic Hybrid Perovskites for Photovoltaic Applications: Recent Advances and Perspectives. *Adv. Mater* **2019**, *29*, 1605005.

12 Fu, H. Review of lead-free halide perovskites as light-absorbers for photovoltaic applications: From materials to solar cells. *Sol. Energy Mater Sol. Cells* **2019**, *193*, 107-132.

13 Chu, L., Ahmad, W., Liu, W., Yang, J., Zhang, R., Sun, Y., Yang, J. & Li, X. Lead-Free Halide Double Perovskite Materials: A New Superstar Toward Green and Stable Optoelectronic Applications. *Nano-Micro Lett.* **11**, 16-34,.

14 Volonakis, G., Filip, M. R., Haghighirad, A. A., Sakai, N., Wenger, B., Snaith, H. J., Giustino, F. Lead-Free Halide Double Perovskites via Heterovalent Substitution of Noble Metals. *J. Phys. Chem. Lett.* **2016**, *7*, 1254-1259.

15 Deng, Z., Wei, F., Sun, S., Kieslich, G., Cheetham, A. K., Bristowe, P. D. Exploring the properties of lead-free hybrid double perovskites using a combined computational-experimental approach. *J. Mater. Chem. A* **2016**, *4*, 12025-12029.

16 McClure, E. T., Ball, M. R., Windl, W. & Woodward, P. M. Cs_2AgBiX_6 (X = Br, Cl): New Visible Light Absorbing, Lead-Free Halide Perovskite Semiconductors. *Chem. Mater.* **2016**, *28*, 1348-1354.

17 Filip, M. R., Hillman, S., Haghighirad, A. A., Snaith, H. J. & Giustino, F. Band Gaps of the Lead-Free Halide Double Perovskites $Cs_2BiAgCl_6$ and $Cs_2BiAgBr_6$ from Theory and Experiment. *J. Phys. Chem. Lett.* **2016**, *7*, 2579-2585.

18 Slavney, A. H., Hu, T., Lindenberg, A. M. & Karunadasa, H. I. A Bismuth-Halide Double Perovskite with Long Carrier Recombination Lifetime for Photovoltaic Applications. *J. Am. Chem. Soc.* **2016**, *138*, 2138-2141.

19 Volonakis, G., Haghighirad, A. A., Milot, R., Sio, W. H., Filip, M. R., Wenger, B., Johnston, M. B., Herz, L. M., Snaith, H. J., Giustino, F. $Cs_2InAgCl_6$: A New Lead-Free Halide Double Perovskite with Direct Band Gap. *J. Phys. Chem. Lett.* **2017**, *8*, 772-778.

20 Luo, J., Wang, X., Li, S., Liu, J., Guo, Y., Niu, G., Yao, L., Fu, Y., Gao, L., Dong, Q., Zhao, C., Leng, M., Ma, F., Liang, W., Wang, L., Jin, S., Han, J., Zhang, L., Etheridge, J., Wang, J., Yan, Y., Sargent, E. H., Tang, J. Efficient and stable emission of warm-white light from lead-free halide double perovskites. *Nature*, **2018**, *563*, 541-545.

21 Wu, C., Du, B., Luo, W., Liu, Y., Li, T., Wang, D., Guo, X., Ting, H., Fang, Z., Wang, S., Chen, Z., Chen, Y., Xiao, L.. Highly Efficient and Stable Self-Powered Ultraviolet and Deep-Blue Photodetector Based on $Cs_2AgBiBr_6/SnO_2$ Heterojunction. *Adv. Opt. Mater.* **2018**, ***6***, 1-7.

22 Gao, W., Ran, C., Xi, J., Jiao, B., Zhang, W., Wu, M., Hou, X., Wu, Z. High-Quality $Cs_2AgBiBr_6$ Double Perovskite Film for Lead-Free Inverted Planar Heterojunction Solar Cells with 2.2 % Efficiency. *ChemPhysChem* **2018**, *19*, 1696-1700.

23 Pan, W., Wu, H., Luo, J., Deng, Z., Ge, C., Chen, C., Jiang, X., Yin, W.-J., Niu, G., Zhu, L., Yin, L., Zhou, Y., Xie, Q., Ke, X. $Cs_2AgBiBr_6$ single-crystal X-ray detectors with a low detection limit. *Nat. Photonics* **2017**, *11*, 1-8.

24 Igbari, F., Wang, R., Wang, Z.-K., Ma, X.-J., Wang, Q., Wang, K.-L., Zhang, Y., Liao, L.-S., Yang, Y. Composition Stoichiometry of $Cs_2AgBiBr_6$ Films for Highly Efficient Lead-Free Perovskite Solar Cells. *Nano Lett.* **2019**, *19*, 2066-2073.

25 Yang, X., Yang, X., Chen, Y., Liu, P., Xiang, H., Wang, W., Ran, R., Zhou, W., Shao, Z. Simultaneous Power Conversion Efficiency and Stability Enhancement of $Cs_2AgBiBr_6$

Lead-Free Inorganic Perovskite Solar Cell through Adopting a Multifunctional Dye Interlayer. *Adv. Funct. Mater.* **2020**, 2001557.

26 Hoye, R. L. Z., Eyre, L., Wei, F., Brivio, F., Sadhanala, A., Sun, S., Li, W., Zhang, K. H. L., MacManus-Driscoll, J. L., Bristowe, P. D., Friend, R. H., Cheetham, A. K., Deschler, F. Fundamental Carrier Lifetime Exceeding 1 μs in $Cs_2AgBiBr_6$ Double Perovskite. *Adv. Mater. Interfaces* **2018,** *5*, 2-9.

27 Nayak, P. K., Mahesh, S., Snaith, H. J. & Cahen, D. Photovoltaic solar cell technologies: analysing the state of the art. *Nat. Rev. Mater.* **2019**, *4*, 269-285.

28 Bartesaghi, D., Slavney, A. H., Gélvez-Rueda, M. C., Connor, B. A., Grozema, F. C., Karunadasa, H. I., Savenije, T. J.. Charge Carrier Dynamics in $Cs_2AgBiBr_6$ Double Perovskite. *J. Phys. Chem. C*, **2018**, *122*, 4809–4816.

29 Hutter, E. M., Gélvez-Rueda, M. C., Bartesaghi, D., Grozema, F. C. & Savenije, T. J. Band-Like Charge Transport in $Cs_2AgBiBr_6$ and Mixed Antimony-Bismuth $Cs_2AgBi_{1-x}Sb_xBr_6$ Halide Double Perovskites. *ACS Omega* **2018**, *3*, 11655-11662.

30 Dang, Y., Tong, G., Song, W., Liu, Z., Qiu, L., Ono, L. K., Qi, Y. Interface Engineering Strategies Towards $Cs_2AgBiBr_6$ Single-Crystalline Photodetectors with Good Ohmic Contact Behaviours. *J. Mater. Chem. C* **2020**, *8*, 276-284.

31 Delor, M. Slavney, A. H., Wolf, N.R., Filip, M. R., Neaton, J. B., Karunadasa, H. I., Ginsberg, N. S. Carrier Diffusion Lengths Exceeding 1 μm Despite Trap-Limited Transport in Halide Double Perovskites. *ACS Energy Lett.* **2020**, *5*, 1337-1345.

32 Gray, M. B., McClure, E. T. & Woodward, P. M. $Cs_2AgBiBr_{6-x}Cl_x$ Solid Solutions – Band Gap Engineering With Halide Double Perovskites. *J. Mater. Chem. C* **20i9**, 6-9.

33 Schmitz, A., Leander Schaberg, L., Sirotinskaya, S., Pantaler, M., Lupascu, D. C., Benson, N., Bacher, G., Fine Structure of the Optical Absorption Resonance in $Cs_2AgBiBr_6$ Double Perovskite Thin Films. *ACS Energy Lett*. **2020**, *5*, 559-565.

34 Kentsch, R., Scholz, M., Horn, J., Schlettwein, D., Oum, K., Lenzer, T. Exciton Dynamics and Electron-Phonon Coupling Affect the Photovoltaic Performance of the $Cs_2AgBiBr_6$ Double Perovskite. *J. Phys. Chem. C* **2018**, *122*, 25940-25947.

35 Bass, K. K., Estergreen, L., Savory, C. N., Buckeridge, J., Scanlon, D. O., Djurovich, P. I., Bradforth, S. E., Thompson, M. E., Melot, B. C. Vibronic Structure in Room Temperature Photoluminescence of the Halide Perovskite $Cs_3Bi_2Br_9$. *Inorg. Chem*. **2017**, *56*, 42-45.

36 Bekenstein, Y., Dahl, J. C., Huang, J., Osowiecki, W. T., Swabeck, J. K., Chan, E. M., Yang, P., Alivisatos, A. P. The Making and Breaking of Lead-Free Double Perovskite Nanocrystals of Cesium Silver-Bismuth Halide Compositions. *Nano Lett*. **2020**, *18*, 3502-3508.

37 Oldenburg, K. & Vogler, A. Electronic Spectra and Photochemistry of Tin (II), Lead (II), Antimony (III), and Bismuth (III) Bromide Complexes in Solution. *Z. Naturforsch*. **1993**, *48b*, 1519-1523.

38 McCall, K. M., Stoumpos, C. C., Kostina, S. S., Kanatzidis, M. G. & Wessels, B. W. Strong Electron-Phonon Coupling and Self-Trapped Excitons in the Defect Halide Perovskites $A_3M_2I_9$ (A = Cs, Rb; M = Bi, Sb). *Chem. Mater*. **2017**, *29*, 4129-4145.

39 Smith, M. D. & Karunadasa, H. I. White-Light Emission from Layered Halide Perovskites. *Acc. Chem. Res*. **2018**, *51*, 619-627.

40 Steele, J. A., Puech, P., Keshavarz, M., Yang, R., Banerjee, S., Debroye, E., Kim, C. W., Yuan, H., Heo, N. H., Vanacken, J., Walsh, A., Hofkens, J., Roeffaers, M. B. J. Giant

Electron-Phonon Coupling and Deep Conduction Band Resonance in Metal Halide Double Perovskite. *ACS Nano* **2018**, *12*, 8081-8090.

41 Ning, W., Wang, F., Wu, B., Lu, J., Yan, Z., Liu, X., Tao, Y., Liu, J.-M., Huang, W., Fahlman, M., Hultman, L., Sum, T. C., Gao, F. Long Electron-Hole Diffusion Length in High-Quality Lead-Free Double Perovskite Films. *Adv. Mater* **2018**, *30*, 1706246.

42 Gao, W., Ran, C., Xi, J., Jiao, B., Zhang, W., Wu, M., Hou, X., Wu, Z. High Quality $Cs_2AgBiBr_6$ Double Perovskite Film for Lead-Free Inverted Planar Heterojunction Solar Cells with 2.2% Efficiency. *ChemPhysChem* **2018**, *19*, 1696-1701

43 Wang, M., Zeng, P., Bai, S., Gu, J., Li, F., Yang, Z., Liu, M. High-Quality Sequential-Vapor-Deposited $Cs_2AgBiBr_6$ Thin Films for Lead-Free Perovskite Solar Cells. *Solar RRL* **2018**, *2*, 1800217.

44 Shockley, W. & Queisser, H. J. Detailed Balance Limit of Efficiency of p-n Junction Solar Cells. *J. Appl. Phys.* **1961**, *32*, 510-519.

45 Kirchartz, T. & Rau, U. Detailed balance and reciprocity in solar cells. *Phys. Status Solidi A* **2008**, *205*, 2737-2751.

46 Liu, Z., Krückemeier, L., Krogmeier, B., Klingebiel, B., Márquez, J. A., Levcenko, S., Öz, S., Mathur, S., Rau, U., Unold, T., Kirchartz, T. Open-Circuit Voltages Exceeding 1.26 V in Planar Methylammonium Lead Iodide Perovskite Solar Cells. *ACS Energy Lett.* **2019**, *4*, 110-117.

47 Mahesh, S., Ball, J. M., Oliver, R. D. J., McMeekin, D. P., Nayak, P. K., Johnston, M. B., Snaith, H. J. Revealing the origin of voltage loss in mixed-halide perovskite solar cells. *Energy Environ. Sci.* **2019**, *13*, 258-267.

48 Stolterfoht, M., Wolff, C.M., Márquez, J. A., Zhang, S., Hages, C. J., Rothhardt, D., Albrecht, S., Burn, P. L., Meredith, P., Unold, T., Neher, D. Visualization and suppression of interfacial recombination for high-efficiency large-area pin perovskite solar cells. *Nat. Energy* **2018**, *3*, 847-854.

49 Wehrenfennig, C., Liu, M., Snaith, H. J., Johnston, M. B. & Herz, L. M. Charge-carrier dynamics in vapour-deposited films of the organolead halide perovskite $CH_3NH_3PbI_{3-x}Cl_x$. *Energy Environ. Sci.* **2014**, *7*, 2269-2275.

50 Johnston, M. B. & Herz, L. M. Hybrid Perovskites for Photovoltaics: Charge-Carrier Recombination, Diffusion, and Radiative Efficiencies. *Acc. Chem. Res.* **2016**, *49*, 146-154.

51 Xiao, Z., Meng, W., Wang, J. & Yan, Y. Thermodynamic Stability and Defect Chemistry of Bismuth-Based Lead-Free Double Perovskites. *ChemSusChem* **2016**, *9*, 2628-2633.

52 Zhang, Z., Yang, G., Zhou, C., Chung, C. C. & Hany, I. Optical and electrical properties of all-inorganic $Cs_2AgBiBr_6$ double perovskite single crystals. *RSC Advances* **2019**, *9*, 23459-23464.

53 Hobson, T. D. C., *et al*. Isotype heterojunction solar cells using n-type Sb_2Se_3 thin films. *Chem. Mater.*, **2020**, *32*, 2621-2630.

54 Cavalcoli, D. & Cavallini, A. Surface photovoltage spectroscopy - method and applications. *Phys. Status Solidi C* **2010**, *7*, 1293-1300.